ADVANCED MATERIALS TECHNOLOGIES

Supporting Information

for *Adv. Mater. Technol.*, DOI: 10.1002/admt.202000386

Electrohydrodynamic Jet Printing of One-Dimensional Photonic Crystals: Part I—An Empirical Model for Multi-Material Multi-Layer Fabrication

*Zahra Afkhami, Brian Iezzi, David Hoelzle, Max Shtein, and Kira Barton**

Supporting Information

Electrohydrodynamic Jet Printing of One-Dimensional Photonic Crystals: Part I, An Empirical Model for Multi-material Multi-layer Fabrication

Zahra Afkhami[1], Brian Iezzi[2], David Hoelzle[3], Max Shtein[2], Kira Barton[1]

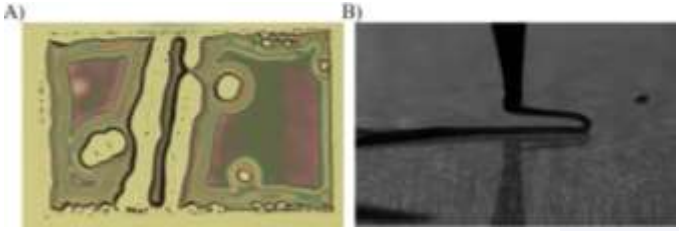

Figure S1. Thin fabrication failures in e-jet printing. A) NOA138 evaporated on the substrate. B) NOA1327 with a low flash point solidifies before landing on the substrate.

A. Material requirements for thin-film fabrication:

Inks should have a boiling temperature higher than the printing environment since evaporation precludes the ink from forming a uniform film on the substrate as can be seen in **Figure S1A**. For example, NOA1348, NOA138, NOA142, NOA144 gradually evaporate on the silicon substrate. Another critical aspect of jetting behavior is understanding the flashpoint of the inks. Specifically, several of the photopolymers investigated had a low flash point and became polymerized before landing on the substrate. For example, we are able to eject both NOA1327 and NOA1328 with a flashpoint of 10 °C from the nozzle tip. However, the jetting stream from both of these inks becomes solidified before reaching the substrate, as presented in **Figure S1B**. This problem has not been observed in other NOA inks with flashpoints larger than 175 °C.

B. Rheological properties of the inks:

Generally, we utilized the manufacturer provided viscosity data. However, we conducted a rheological study to determine the viscosity dependence on the shear rate for Loctite3526. The manufacturer-supplied value of 17,500 cP was confirmed at shear rates up to 200 s^{-1}. However, higher shear rates led to a decrease in the apparent viscosity. Future work we will focus on the rheological behavior of all the inks under relevant shear rates encountered while printing.

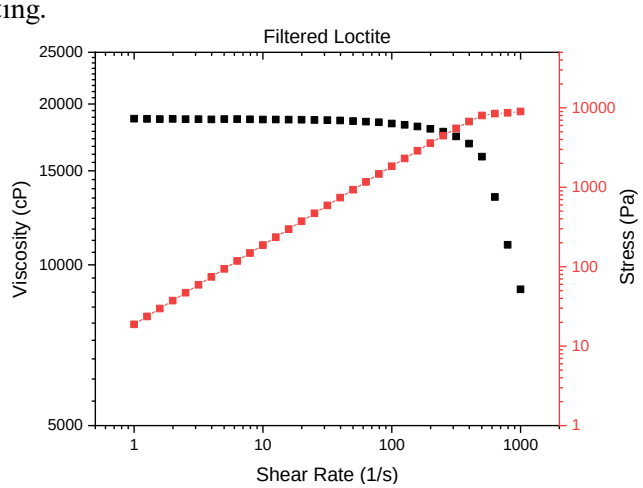

Figure S2: Experimental results for viscosity versus shear rate for Loctite3526.

C. SSE and LST Measurements:

The static contact angle of probe liquids is used to calculate SSE values via the methods of Owens-Wendt and Wu. These methods are chosen based on the wide use of the Owens-Wendt method and the accuracy of the Wu method in measuring low surface energy polymers. They differ primarily in the calculation of the mean of the polar and dispersive components of the energy, with the Owens-Wendt method using a geometric mean and Wu using a reciprocal mean;

$$\text{Owens-Wendt: } \gamma_{ls} = \gamma_s + \gamma_l - 2\left(\sqrt{\gamma_s^D \gamma_l^D} + \sqrt{\gamma_s^P \gamma_l^P}\right)$$
$$\text{Wu: } \gamma_{ls} = \gamma_s + \gamma_l - 4\left(\frac{\gamma_s^D \gamma_l^D}{\gamma_s^D + \gamma_l^D} + \frac{\gamma_s^P \gamma_l^P}{\gamma_s^P + \gamma_l^P}\right) \quad (3)$$

where γ_{ls} is the liquid-solid interfacial tension, γ_s is the SSE, γ_l is the LST, γ_l^D is the dispersive portion of the liquid surface tension, γ_l^P is the polar portion of the liquid surface tension, γ_s^D is the dispersive portion of the solid surface energy, and γ_s^P is the polar portion of the solid surface energy. Using the Young-Dupre equation, which relates these quantities to the contact angle on the surface, it is possible to calculate γ_s^D and γ_s^P. Table S2 summarizes the contact angles measured and the resulting solid surface energies. The values listed in the main text are taken as the average of the Owens-Wendt and Wu methods (listed in the far-right column).

Table S1: *Density and liquid surface tension of all inks studied in this work.*

Ink	Density (g cm^{-3})	γ_l (mN m^{-1})
NOA170	1.94±0.11	37.3±2.1
Loctite3526	0.94±0.04	25.1±2.1
NOA1369	1.16±0.07	14.5±0.9
NOA13775	1.40±0.04	19.4±0.4
NOA13825	1.57±0.21	21.1±2.5
NOA1348	1.50±0.15	18.6±1.8
NOA138	1.02±0.03	19.3±0.7
NOA142	1.04±0.16	20.7±2.9
NOA144	0.90±0.18	19.1±3.3

Table S2: *Static contact angles and solid surface energy of all primary and secondary substrates. All contact angles are in degrees and all solid surface energies are in mN m^{-1}.*

			Owens-Wendt			Wu			
Substrate	θ_s^{Water}	θ_s^{DIM}	γ_s^P	γ_s^D	γ_s^T	γ_s^P	γ_s^D	γ_s^T	Average
Silicon/Native Oxide	27.1±1.0	52.0±3.8	46.6	18.5	65.1	38.6	28.8	67.4	66.3±0.8
NOA170	66.8±0.3	35.5±3.9	10.5	34.5	45.0	36.5	15.1	51.6	48.3±1.4
Loctite3526	109.8±11.6	79.9±4.9	0.4	17.3	17.7	1.7	19.5	21.2	19.4±2.6
NOA1369	109.8±0.8	90.3±1.3	1.3	11.4	12.7	3.5	14.5	18.0	15.3±0.5
NOA13775	104.4±4.6	81.2±3.3	1.6	15.4	17.0	4.1	17.8	22.0	19.5±2.1
NOA13825	109.0±1.5	84.0±3.8	0.9	14.6	15.5	2.8	17.2	20.0	17.7±1.7
NOA1348	118.7±0.5	98.9±0.6	0.5	8.5	9.0	1.7	12.2	13.9	11.5±0.2
NOA138	111.9±0.3	92.3±3.8	1.1	10.7	11.8	3.1	13.8	16.9	14.3±1.3
NOA142	113.5±5.8	90.2±4.8	0.6	12.0	12.6	2.1	15.1	17.2	14.9±2.3
NOA144	108.8±1.1	91.8±5.8	1.8	10.4	12.2	4.2	13.7	17.9	15.1±1.9

A. Contact angle measurement at the macroscale

Comparing the experimental results provided in **Figure 4B** and **Figure S3A**, it is observed that microscale contact angle measurements are not in agreement with the macroscale contact angle measurements. For instance, microscale contact angle measurements return a low value of the contact angle related to the NOA170 – filtered Loctite3526 combination (θ=13º±0.8º), indicating that this combination is favorable for forming uniform films. However, at the macroscale, droplets of NOA170 on a spin-coated film of filtered Loctite3526 demonstrate one of the highest contact angles at θ=108.3º±0.8º. With the viscosity and liquid surface tension of the NOA170 ink held constant, the variables that differ between the two deposition systems are the heterogeneity of the solid surface energy and the velocity with which the droplet is impacting the surface.

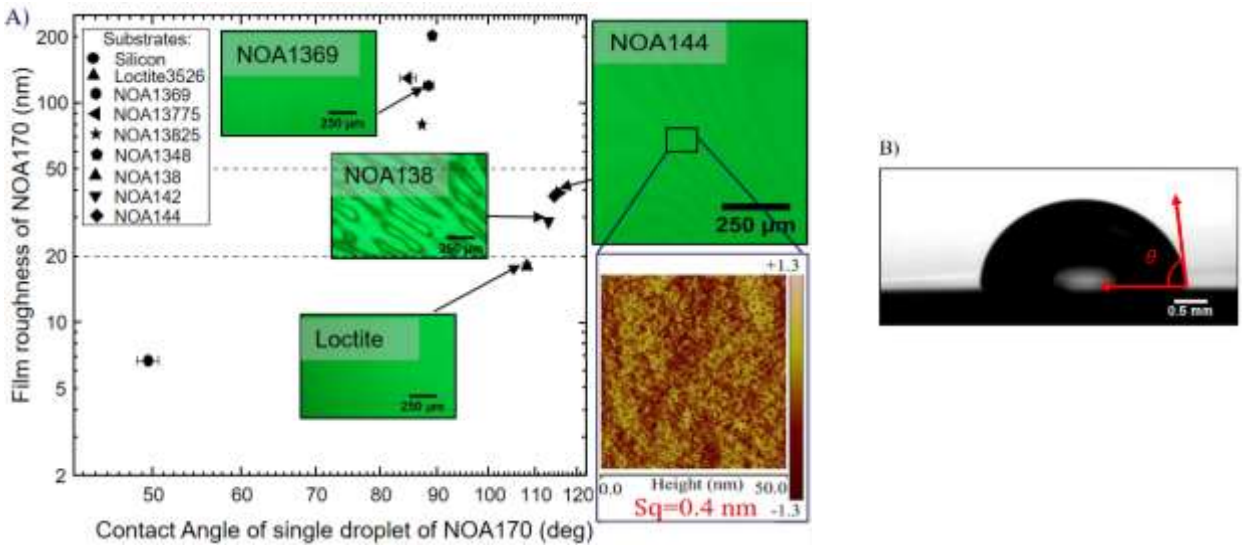

Figure S3. Correlation between contact angle measurement at the macroscale and material behavior at the microscale. A) Contact angle of NOA170 as a build material on various substrates at the macroscale (with test droplets ~1-3 mm) versus roughness of an NOA170 films (60 µm×60 µm) at the microscale on various substrates. B) Contact angle measurement at the macroscale using a goniometer with droplet diameter ranging from 1-3 mm.

Previous reports have shown that surface heterogeneity can lead to significant changes in SSE values and an artificial increase or decrease in the contact angle of droplets on a surface depending on the length scale of the heterogeneity and the size of probe droplets used[37]. Furthermore, high deposition velocities with the e-jet process coupled with high viscosity inks (>5,000 cP for NOA170) could, at the microscale, overcome surface energetic limitations apparent at the macroscale [38]. Specifically, a high viscosity ink may flatten out under high deposition velocities. Optical micrographs utilizing a 532 nm bandpass filter were taken of the spun coat layers of NOA138, NOA144, Loctite3526, and NOA1369. The filter allows the topology of these layers to be investigated at longer length scales. It was found that NOA138 and NOA144 both demonstrated irregular surface topologies while NOA1369 and Loctite3526 were both relatively smooth. Referencing the behavior of the same materials at the microscale, it can be seen that the heterogeneous topology exhibited in NOA138 and NOA144 could artificially increase the contact angle. Specifically, AFM measurements of NOA144 with a scan area <2500 µm^2 indicate extremely smooth surfaces (s_q < 1 nm), but this does not hold for larger areas (indicated by interference patterns in the optical micrograph taken by an optical microscope). Interestingly, this does not explain the merging quality between NOA170 – filtered loctite3526. This could potentially be explained by chemical heterogeneity in the sample, which can lead to pinning of the droplet.

The work of cohesion, W_C, of a particular liquid is defined as the work per unit area needed to divide that homogeneous liquid from itself. In contrast, the work of adhesion, W_A, is defined as the amount of work needed to separate a liquid from a solid surface of another material;

$$W_C = 2\gamma_l \quad (4)$$

$$W_A = \gamma_l(1 + \cos\theta) \quad (5)$$

$$R = \frac{W_A}{W_C} = \frac{(1+\cos\theta)}{2} \quad (6)$$

where θ is the angle the liquid makes with the surface. In general, more energy is required to separate a liquid from itself (W_C) than from a solid surface (W_A). Thus, the R ratio in Equation 6 is typically less than 1 and has been used previously to show that liquid/surface combinations with higher R ratios have a higher chance of merging to form a uniform line [27]. Another benefit to using this ratio is that it is solely dependent on the contact angle a specific liquid makes with a specific substrate.

Tables S3 and **S4** show material interactions at the micro and macroscale. White cells indicate full merging, light gray cells indicate partial merging, and dark gray cells indicate no merging at the microscale. Elucidating the actual discrepancy between microscale and macroscale measurements could potentially be addressed via a future study using picoliter-sized droplets to determine the microscale surface energy (γ_l and γ_s at the

microscale) [39]. As mentioned before, material merging at the microscale is a trade-off between the contact angle at the microscale, the surface energy of the previous layer, and the surface tension of the build material. The zero contact angles in **Table S3** mean complete wetting that was observed at the macroscale. It should be noted that NOA138, NOA142, and NOA144, quickly evaporate on the substrate and we could not measure their contact angles. To measure the contact angle of NOA 170 on these materials, we spin-coated the samples in a glove box and cured them immediately to reduce the evaporation rate, before e-jet depositing droplets of NOA170 on top of them.

In summary, a material combination with a low micro-contact angle (< 15°) and high SSE and LST values such that $\gamma_l<\gamma_s$ has a higher proclivity to merge. We can quantify all of these parameters by comparing the value of R for all material combinations. Based on results in Tables S3 and S4, and Figures 3 and 6A, full merging at the microscale happens with $0.987<R<1$, partial merging with $0.952<R<0.97$, and failure to merge with $R<0.952$.

Table S3: *Contact angle and surface energetic measurements of various low index (n_L) photopolymers on NOA170 (n_H) films at the macro and microscale. $\overline{g}$ and s_q are the average thickness and RMS roughness of the e-jet printed films.*

Build material	γ_l	γ_s	W_C	**Micro measurement (n_L droplet on n_H surface)**			**Macro measurement (n_L droplet on n_H surface)**			**n_L film on n_H surface**	
				$\theta°$	W_A	R	$\theta°$	W_A	R	$\bar{g}$(nm)	s_q(nm)
Loctite3526 (filtered)	25.1		50.14	11.4±3.2	49.6	0.990	27.7±1.5	47.2	0.943	130.7	8.1
NOA1369	14.5		29.06	6±2.2	28.9	0.997	33.2±1	26.7	0.918	85.5	5.4
NOA13775	19.4	48.3	38.8	7.12±1.1	38.6	0.996	92.6±5	18.5	0.477	123.3	8.7
NOA13825	21.1		42.1	7.8±0.9	41.9	0.995	88.3±7.6	21.7	0.515	100.6	8.6
NOA138	19.3		38.6	-	-	-	0	38.6	1	280.5	100.2
NOA142	20.7		41.48	-	-	-	0	41.4	1	250.6	130.6
NOA144	19.1		38.18	-	-	-	0	38.1	1	280.3	140.1

Table S4: *Contact angle and surface energetic measurements of NOA170 (n_H) on various low index surfaces (n_L) at the macro and microscale. $\overline{g}$ and s_q are the average thickness and RMS roughness of the e-jet printed films.*

Substrate	γ_l	γ_s	W_C	**Micro measurement (n_H droplet on n_L surface)**			**Macro measurement (n_H droplet on n_L surface)**			**n_H film on Silicon / n_L surface**	
				$\theta°$	W_A	R	$\theta°$	W_A	R	$\bar{g}$(nm)	s_q(nm)
Silicon		66.3		9±3.2	74.1	0.993	49.5±1.1	61.5	0.825	85.2	6.7
Loctite3526 (filtered)		19.4		13±0.8	73.6	0.987	108.3±0.8	25.6	0.343	199.1	18.1
NOA1369		15.3		34.5±4.7	68.0	0.912	88.3±0.9	38.4	0.515	290.2	120.2
NOA13775	37.3	19.5	74.6	34.5±5.8	68.1	0.912	84.7±1.4	40.8	0.547	200.6	130.2
NOA13825		17.7		45.3±12.4	63.5	0.852	87.1±0.3	39.2	0.525	210.3	80.2
NOA1348		11.5		29.5±5.7	69.8	0.935	89.0±0.5	37.9	0.509	295.8	202.7
NOA138		14.3		25.1±5.4	71.1	0.952	113.1±0.1	22.7	0.304	193.1	28.9
NOA142		14.9		20.2±1.6	72.3	0.96	115.7±0.1	21.2	0.284	195	39.1
NOA144		15.1		19.63±2.1	72.4	0.97	114.6±0.3	21.9	0.294	152.5	37.8

References

[37] J. N. Israelachvili, M. L. Gee, *Langmuir* **1989**, *2*, 288.
[38] C. P. Pannier, M. Diagne, I. A. Spiegel, D. J. Hoelzle, K. Barton, *J. Manuf. Sci. Eng.* **2017**, *139*, 111008.
[39] M. Taylor, A. J. Urquhart, M. Zelzer, M. C. Davies, M. R. Alexander, *Langmuir* **2007**, *23*, 6875.